Developmental Biology 450 (2019) 76–81

Contents lists available at ScienceDirect

Developmental Biology

journal homepage: www.elsevier.com/locate/developmentalbiology

Apical constriction is necessary for crypt formation in small intestinal organoids

Leonie Hartl, Guizela Huelsz-Prince, Jeroen van Zon, Sander J. Tans *

AMOLF, Science Park 104, 1098 XG Amsterdam, the Netherlands

ARTICLE INFO

Keywords:
Small intestine organoids
Crypts of Lieberkühn
Apical constriction
Non-muscle myosin II
Blebbistatin

ABSTRACT

Small intestinal organoids have become an important tool to study crypt homeostasis, cell fate dynamics and tissue biomechanics. Yet, the mechanisms that drive the budding of crypts from the smooth organoid epithelium remain incompletely understood. Locally enhanced proliferation has been suggested to induce tissue buckling and crypt initiation. Here we report that changes in cell morphology play a crucial role in crypt formation. Crypt formation is preceded by local epithelial thickening, apicobasal elongation, and apical narrowing, resulting in a wedge-like cell-shape, followed by apical evagination and crypt outgrowth. Myosin II activity is found to coincide with apical constriction of cells, while inhibition of myosin suppresses apical constriction and bud formation. The data suggest that myosin-driven apical constriction is a key driving force of bud initiation in small intestinal organoids.

1. Introduction

The small intestinal epithelium is among the most rapidly regenerating tissue in mammals (Valéry et al., 2011). To maximize its nutrient- and fluid absorptive capacities, it is covered with finger-like protrusions termed villi. In-between the villi, the crypts of Lieberkühn are found (Shyer et al., 2013). Here, the stem cells reside and replenish the epithelium. The stem cells are interspersed by Paneth cells which maintain a sterile crypt environment and signal factors to regulate stemness and linage specification of stem cell progeny (Clevers and Bevins, 2013; Clevers, 2013; Sato et al., 2011). In humans crypts develop around week 20 of gestation while in mice, they develop at 1–2 weeks after birth (Chin et al., 2017). Crypt formation is not confined to the (post-) embryonic evolution of the small intestine. For instance, upon damage by disease, irradiation treatment or environmental conditions, the epithelium can be re-built by an expanding stem cell population giving rise to stem cell crypts by crypt fission (Carulli et al., 2014). Small intestinal organoids have been used to study intestinal stem cell crypts *in vitro*, and constitute a platform that allows for genetic manipulation and microenvironmental changes (Gjorevski et al., 2016). They have provided insight into crypt homeostasis (Snippert et al., 2010; Sato et al., 2011), signaling pathways (Gregorieff et al., 2015; VanDussen et al., 2012), cell fate dynamics (Heuberger et al., 2014), cell- and tissue biomechanics (Buske et al., 2012), as well as tumorigenesis (Fatehullah et al., 2013) and cell-inherent intestinal diseases (Zhao et al., 2015). The mechanisms involved in crypt formation or budding in organoids remain incompletely understood. Crypt formation has been modeled as a mechanical buckling phenomenon driven by spatial differences in proliferative rates (Nelson et al., 2011a). Itzkovitz et al. found that so-called 'bang-bang control' of cell proliferation, in which the system switches once from symmetric to asymmetric division, is the most efficient way to build up a mature crypt (Itzkovitz et al., 2012), suggesting that specific proliferation patterns are driving forces of crypt development. Cell-based computational modeling indicated that small changes in epithelial curvature caused by enhanced proliferation can initiate nascent crypt domains and promote Paneth cell differentiation, with Paneth cells in turn stabilizing crypts by inducing local tissue curvature (Buske et al., 2012). Whether and how changes in cell morphology play a role in crypt formation remains poorly addressed. Cell morphological changes have been shown to accompany and guide a manifold of tissue morphological transition, ranging from tissue patterning during embryogenesis (Paluch and Heisenberg, 2009), somite compartmentalization (Pilot and Lecuit, 2005; Saias et al., 2015), organogenesis, neural tube formation, tissue branching (Varner and Nelson, 2014) and gland development (Ewald et al., 2008), right up to wound healing (Razzell et al., 2014) and tissue regeneration in the adult organism. Here, we use small intestine organoids to study the role of cumulative epithelial cell shape changes in crypt formation.

* Corresponding author.
E-mail address: tans@amolf.nl (S.J. Tans).

https://doi.org/10.1016/j.ydbio.2019.03.009
Received 9 July 2018; Received in revised form 26 February 2019; Accepted 14 March 2019
Available online 23 March 2019

2. Results

2.1. Stages of crypt formation

To study cell shape during crypt formation, we imaged organoids at different stages of development. When single cells or dissociated crypts are seeded in Matrigel®, they self-assemble into cystic structures or seal up at the fractured site respectively, with the apical membrane facing the lumen of the cyst (Fatehullah et al., 2013). Microscopy imaging of budding organoids (N = 85) indicated different stages of cell- and organoid morphologies that we categorized into four types (Fig. 1). The timing of crypt formation is variable, and can be completed in one or several days. Generally, around 12 h after crypt dissociation and seeding, the cystic organoid walls are of uniform thickness and consist of a monolayer of cells (Fig. 1A, E). 12 h later the cyst loses symmetry and thickens on one side while the lumen of the organoid remains spherical. On the thickened side, the apical side of the cells have become narrower, with the cell being more elongated and wedge-shaped (Fig. 1B, F). The cells also appear tilted, with their apical side leaning towards the thickest point (Fig. 1B, F). At the third stage, 1–2 days after dissociation, the observed cell shape changes are more accentuated and the lumen shows a first evagination (Fig. 1C, G). Next, the crypt rapidly matures and grows away from the lumen (Fig. 1D, H). The characteristic wedged shape and tilt of cells are conserved in the tip of the mature crypt.

2.2. Cellular elongation, tilt, and wedge-shape

To quantify cell morphology and morphogenesis, we defined the apico-basal and lateral axis of the cells as illustrated in Fig. 2A and B. Cellular tilt was defined as the angle between these two axis, minus 90° (Fig. 2B), and cellular elongation as the ratio between the lengths of the two axis. The apical index was defined as the ratio between the basal and apical widths of the cells, and hence quantified the wedge-shape. These features were quantified at the budding stage (Fig. 1C, G) as a function of cell position from cross-sections of organoids (N = 10, Fig. 2C–E).

The data show that tilt, elongation, and wedge shape are confined around the bud center (Fig. 2C–E), consistent with a local apical constriction (Sawyer et al., 2010; Martin and Goldstein, 2014). Tilt is not significant for the first 1–2 cells away from the bud center, then peaks to about 47°, and remains significant up to 8 cells away from the bud center on either side (Fig. 2C). Elongation and wedge shape are more confined, and extend to about 3 cells on either side of the bud center (Fig. 2D and E). Cells in the bud elongate the most, with an apico-basal axis reaching up to twice the length of the lateral axis (Fig. 2D). The apical index peaks to over 10 in the bud center (Fig. 2E), indicating that the cells are over an order of magnitude narrower at the apical side than the basal side. Further away from the bud center at the opposite side of the organoid, we find that some cells are stretched laterally and have become more wide than long, resulting in a negative apical index (Fig. 2A, E).

2.3. Myosin activity

Apical constriction has been observed in a number of embryonic developmental processes including gastrulation and neural tube closure in *Echinoidea*, *Xenopus laevis*, *Drosophila melanogaster* and *Caenorhabditis elegans*, furrow formation and dorsal closure in *Drosophila melanogaster*, wound healing in *Xenopus laevis* and vertebrate tube formation (Sawyer et al., 2010). Each of these processes is accompanied and presumably guided by phosphorylation and subsequent activation of non-muscle myosin which induces contraction of the apical filamentous actin (F-actin) network of cells. The force generated by this contraction is transferred to neighboring cells via actin filaments attaching to adherens junctions which thereby form a supra-cellular contractile network (Martin and Goldstein, 2014; Jodoin et al., 2015).

To assess the involvement of myosin in apical constriction in budding organoids, we localized and quantified its activity on the subcellular level. We labeled phosphorylated myosin light chain using immunofluorescence (Fig. 3A) and quantified the fluorescence intensity along the organoid apical surface (Fig. 3B and Supplementary Fig. S1A). Myosin activity is highest at the center of the bud, and decreases over a distance of 10 μm which corresponds to the apical surface of about 3 cells on either side of the bud center – a similar distance as observed for wedge-shape and elongation (Fig. 2D and E). If myosin activity is required for apical constriction, then higher myosin levels should correlate with stronger constriction. Consistently, we find that the mean cellular apical fluorescence intensity is higher in constricted cells that have a smaller

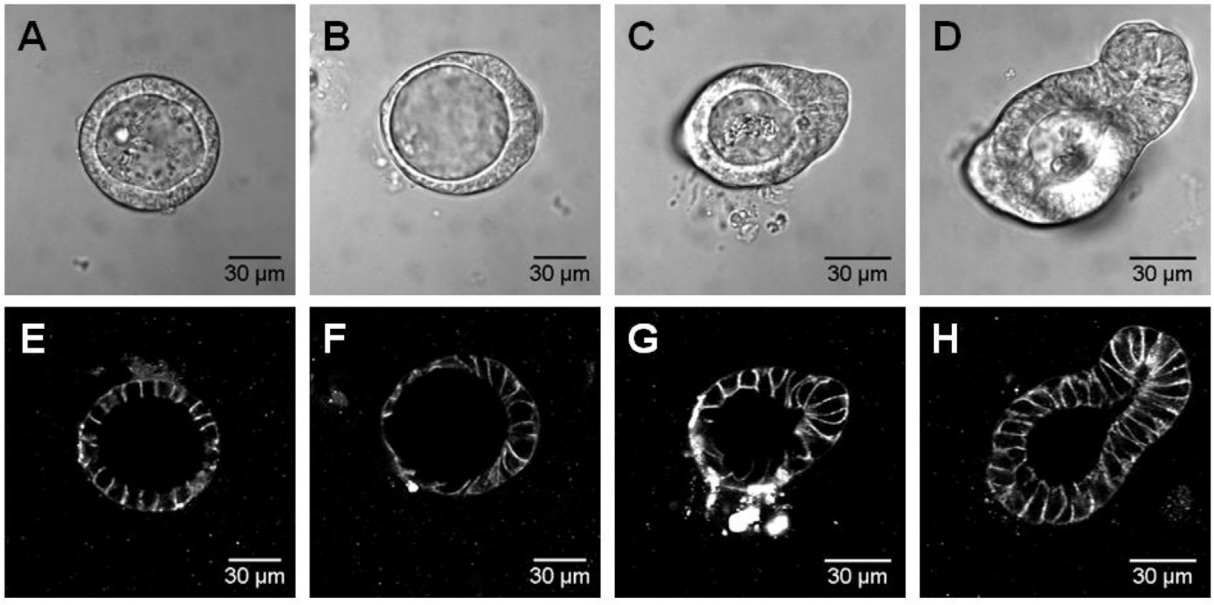

Fig. 1. Stages of crypt budding in small intestine organoids. (A–D) Cross-sectional bright field images of individual organoids at different time points after passage by crypt dissociation. Magnification: 40×. (E–H) Cross-sections of the respective organoid with a plasma membrane stain. (A+E) Self-assembly into a symmetric cyst, 12 h after crypt dissociation. (B+F) Loss of symmetry, the cyst bulges out, 24 h. (C+G) A bud forms at the thickened site, 1–2 days. (D+H) The bud grows away from the cyst to develop a mature crypt, 1–2 days.

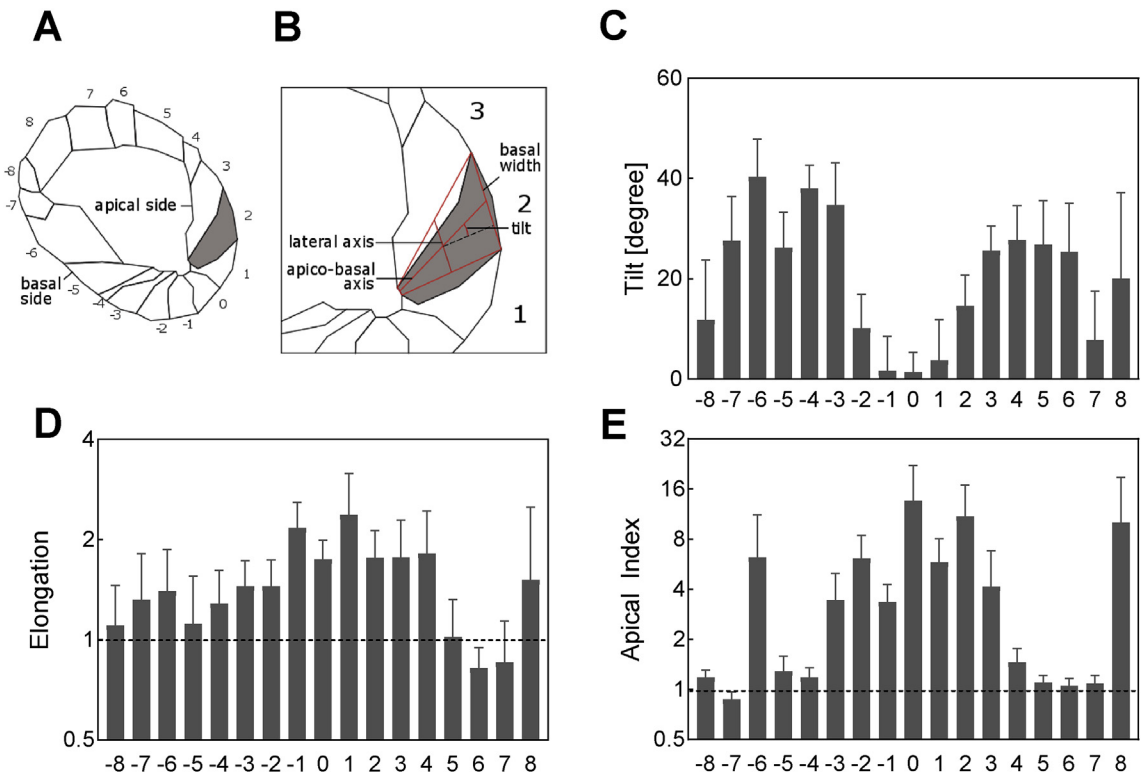

Fig. 2. Cell shape changes suggest apical constriction. (A) Schematic representation of a budding organoid. Cells are numbered starting at the center of the nascent bud. (B) Morphological parameters used to calculate tilt, elongation and constriction. (C–E) X-axis indicates the cell number, with 0 the bud center. N = 10 organoids. (C) Histogram of the cellular tilt, defined as the angle between the cell's lateral and apico-basal axis minus 90°. (D) Histogram of the cellular elongation, defined as the ratio between the lengths of the apico-basal and lateral axis. Dashed line marks cuboidal cells. (E) Histogram of the apical index, defined as the basal width over the apical width of the cells. Dashed line marks cuboidal cells.

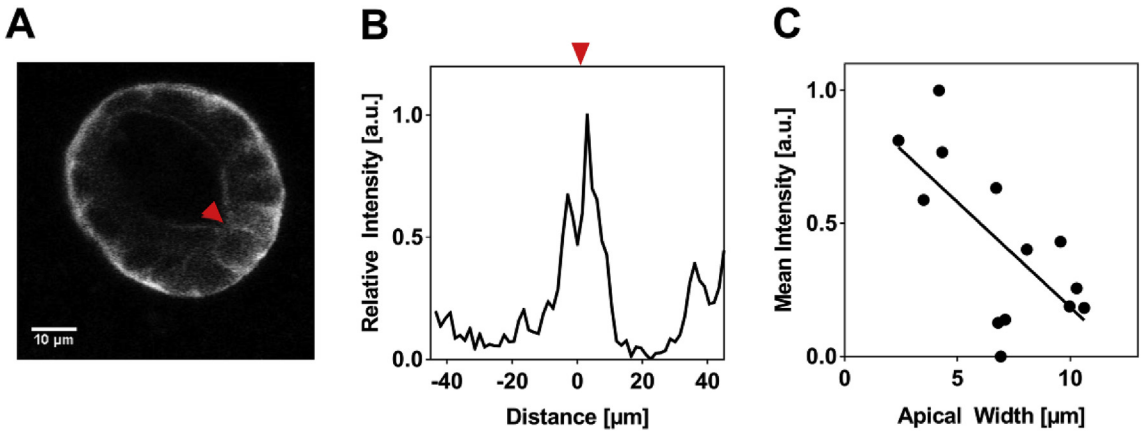

Fig. 3. Enhanced myosin activity correlates with constriction of the apical membrane. (A) Phosphorylated myosin signal in a budding organoid (anti-myosin light chain antibody). Red arrowhead indicates the center of the bud. (B) Fluorescence intensity along the apical surface of budding organoids shows elevated activity at the budding site. (C) Myosin signal intensity per cell, plotted against the cellular apical width, showing myosin activity increasing with apical narrowing. Myosin signal intensity corresponds to the mean intensity per cell, as defined by the total intensity per cell divided by the apical width of the cell.

apical width (Fig. 3B and C and Supplementary Fig. S1B, Pearson correlation coefficient $r = -0.6$ with $p < 0.001$ for 70 cells from 4 organoids).

2.4. Myosin inhibition

To further probe the role of myosin, we used the myosin inhibitor blebbistatin. Blebbistatin has been used at low doses of 10 µM to enhance the survival of single stem cells and dissociated crypts in culture (Zhao et al., 2015). At higher concentrations of 50–100 µM, it has been shown to inhibit apical constriction in different developmental processes (Kinoshita et al., 2008; Borges et al., 2011). We prepared medium containing 100 µM blebbistatin, though observed blebbistatin crystallization indicated that actual concentrations were lower. We added the medium to organoids at different developmental stages, and refreshed it daily. Furthermore, we note that media with blebbistatin concentrations of up to 20 µM did not show an effect. First, blebbistatin was added to cysts not yet showing buds (as in Fig. 1A, approximately 12 h after seeding). After 24 h, we then did not observe apically constricted, elongated or tilted cells (Supplementary Figs. 2A and B). In contrast, the latter is observed in

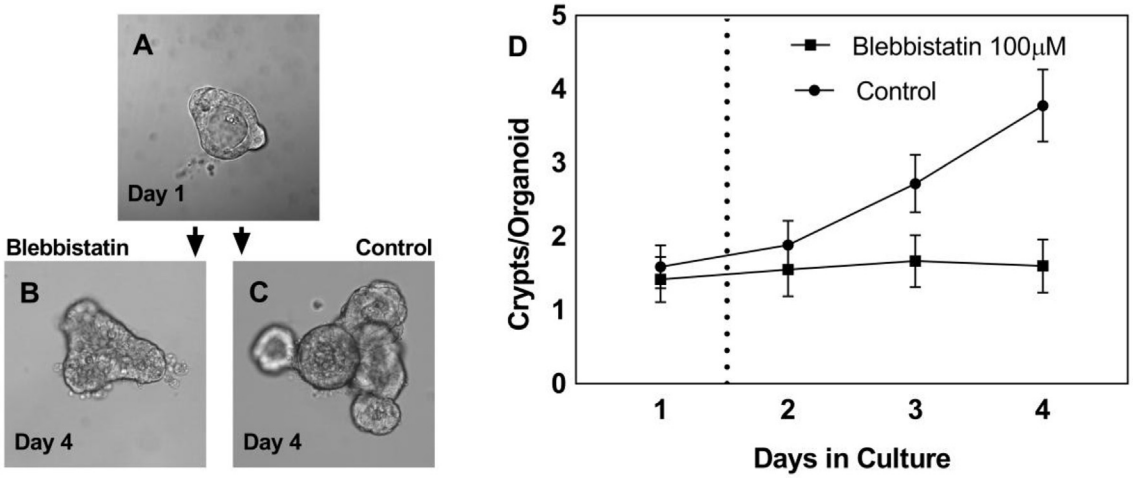

Fig. 4. Blebbistatin treatment halts bud-initiation in organoids. (A) Example of a budding organoid, 24 h after crypt dissociation. (B) Blebbistatin-treated (100 μM) organoids show few crypts after four days, while the crypt necks have widened. (C) Untreated organoids show an increase in crypt number after four days in culture, and normal narrow crypt necks. (D) Control organoids show a more than two-fold increase in crypt number, while blebbistatin-treated organoids show no increase in crypt count until day four. Dashed line indicates the first addition of blebbistatin. Fresh blebbistatin is added every 24 h.

untreated organoids (Supplementary Fig. 2C). We find that within untreated organoids, about 50% of the imaged cells (N = 154) have an apical index above 3, while this is the case for less than 2% of the cells (N = 90) in the blebbistatin-exposed organoids. These data suggest that blebbistatin suppresses apical constriction on the cellular level.

Second, blebbistatin was added to already budding cysts (as in Fig. 1C, approximately 1–2 days after dissociation, Fig. 4A). After four days, we observed a significant difference in de novo crypt formation (Fig. 4B and C): Control organoids showed a more than two-fold increase in crypt number from day 2 to day 4 while blebbistatin-treated organoids failed to induce new buds or crypts (Fig. 4D). We note that blebbistatin can also inhibit growth, which in turn could affect crypt formation. At the same time, the blebbistatin-treated organoids were observed to increase in size (Fig. 4A and B), indicating that growth continued, even if at a lower rate. However, we also observed changes in the bud features. Specifically, buds in blebbistatin-treated organoids were smooth in terms of shape, lacking sharp features, and showing wide necks (Fig. 4B). Prior to the treatment, the envelope of the buds did display distinct angles (Fig. 4A, right, base of the bud), while more mature crypts showed narrow necks with distinct angles as well (Fig. 4C). These observations suggested that blebbistatin modified (relaxed) already formed and grown bud-features, consistent with its role as a myosin inhibitor.

3. Discussion

It has been suggested that intestinal crypt formation is initiated by locally enhanced cell proliferation (Itzkovitz et al., 2012) or by biomechanical processes like growth-induced buckling (Nelson et al., 2011b). While these mechanisms may also play a role in crypt formation, the cell morphological changes and myosin activity observed here indicate that apical constriction is central to the initial budding phase.

3.1. Apical constriction morphometrics

The observed apical constriction is symmetric with respect to the bud center. This is evidenced by the symmetric elongation, tilt, constriction, and myosin activity profiles, suggesting highest contraction forces localized at the bud center. These forces appear to affect not only contracting cells, but also neighboring ones beyond 3 cells away from the bud center, which do show tilt but no significant wedge-shape or elongation. Indeed, one expects that local contraction and resulting wedge-shape to induce a tilt in neighboring cells, given the mechanical constraints of an epithelial layer and its surrounding matrix. Consistently, we find that cellular tilt is indeed also visible in previously reported imaging of apically constricting cells in *Drosophila melanogaster* ventral furrow formation, and of bottle cells initiating involution of the blastopore in *Xenopus laevis* (He et al., 2014; Lee and Harland, 2007a). Cell elongation can accompany apical constriction and convert cuboidal cells into columnar ones (Suzuki et al., 2010). Different approaches have been followed to elucidate whether elongation is a mere side effect of apical constriction or rather an independent process (Lee and Harland, 2007b). In the data presented here, cells at the nascent bud display increases in both the apical index and elongation. While these observations do not address causality, they do show that elongation and constriction are correlated. Generally, the wedged shape of constricting epithelial cells is thought to result from contractile forces along the apical cell membrane (Martin et al., 2010). Consistently, cells near the organoid bud centers have the smallest apical dimensions while cells more distant from the bud center exhibit weaker constriction. This suggests a gradient of myosin activity, which we indeed also observed. The correlation between myosin activity and apical width further supports the idea that myosin activity underlies the observed apical constriction.

3.2. The role of myosin in crypt formation

We found that blebbistatin can suppress but not reverse apical constriction in organoids. When treating organoids before the budding stage, they failed to induce apical constriction, bud formation and crypt outgrowth. Confocal images with membrane markers confirm that the characteristic features of apical constriction are not found in treated organoids at a time where control organoids have initiated well-defined buds. Thus, blebbistatin can inhibit apical constriction on the cellular level. Treating organoids with nascent buds on the other hand, revealed that crypts can grow out during blebbistatin treatment, presumably by enhanced proliferation. Yet, the total crypt count did not increase. Furthermore, we observed that blebbistatin-treated organoids and their crypts become less well-defined. Specifically, the crypt necks that are normally narrow had now widened. Untreated organoids on the contrary initiate new, well-defined crypts and their number doubles every two days. These data indicate that myosin activity is not only involved in bud initiation but also in shaping and maintaining other morphological features. Consistently, we find that other features such as wedge-shape are maintained throughout crypt development and in the mature crypt.

4. Conclusion

By analyzing the shape of cells in organoids at different stages of development we show that apical constriction is a key feature of organoid crypt formation. Immunofluorescence and targeted inhibition of myosin are consistent with this hypothesis, while other mechanisms such as enhanced proliferation contribute to the maturation of crypts. Revealing the mechanism of crypt formation and maintenance is relevant to advance our understanding of fetal and neonatal tissue development as well as the regeneration and repair following severe and mild injuries such as irradiation- and chemotherapy induced crypt and stem cell loss.

5. Experimental procedures

5.1. Organoid culture

Stem cell crypts were obtained from 4-6-week-old C57BL/6 mice as previously described by Sato et al. (Sato and Clevers, 2012). Dissociated crypts or single cells were embedded in Matrigel® and covered with medium (EGF (50 ng/ml, Life Technologies), Noggin (100 ng/ml, Prepotech), R-spondin 1 (500 ng/ml, Prepotech), n-Acetylcysteine (1 mM, Sigma-Aldrich), N2 supplement (1×, 10 μL/mL, Life Technologies), B27 supplement (1×, 20 μL/mL, Life Technologies), Glutamax (2 mM, Life Technologies), HEPES (10 mM, Life Technologies), Penicilin/Streptomycin (100 U/ml 100 μg/ml, Life Technologies) in Advanced DMEM/F-12 (Life Technologies). Mature organoids were mechanically disrupted by drawing them through a thinned glass pipette.

5.2. Immunostaining and image acquisition

For myosin light chain staining, organoids were fixed using 3.7% formaldehyde in TBS, permeabilized with 0.2% Triton X-100 in TBS and blocked with 3% BSA, 100 mM Glycine and 0.1% Tween-20 in TBS. Primary antibodies (rabbit, 1:400, Abcam #ab2480) and secondary ones (donkey-anti-rabbit, 1:1000, Abcam #ab175649) were diluted in blocking solution.

Cell membranes were stained with CellMask™ Orange (1:1000, Thermofisher) or CellMask™ Deep Red (1:1000, Thermofisher).

Organoids were imaged using a confocal laser scanning microscope (Eclipse Ti; Nikon Instruments) with a 40× oil immersion objective (NA = 1.30). ImageJ was used for fluorescence image analysis.

5.3. Morphometrics

The outline of each cell is determined manually using polygons in Adobe Illustrator. The apical and basal width of a cell are approximated by the distance between the most apical and most basal contact points of neighboring cells. The cell's apico-basal axis is drawn between the midpoints of the apical and basal border, the lateral axis is drawn between the midpoints of the lateral membranes.

5.4. Myosin inhibition

For myosin inhibition blebbistatin (Enzo, BML-El315-0005) was dissolved in DMSO to obtain a 10 mM stock solution. Blebbistatin-containing medium was replaced every day due to blebbistatin crystallization. The specificity of blebbistatin for myosin light chain in organoids has been validated by presence of multinucleate cells upon treatment.

Acknowledgements

Work in the groups of S.J.T. and J. van Zon are supported by the Netherlands Organization for Scientific Research (NWO). We thank J. Beumer for critical reading of the manuscript.

Appendix A. Supplementary data

Supplementary data to this article can be found online at https://doi.org/10.1016/j.ydbio.2019.03.009.

References

Borges, R.M., Lamers, M.L., Forti, F.L., Santos, MF dos, Yan, C.Y.I., 2011. Rho signaling pathway and apical constriction in the early lens placode. Genesis 49 (5), 368–379. https://doi.org/10.1002/dvg.20723.

Buske, P., Przybilla, J., Loeffler, M., et al., 2012. On the biomechanics of stem cell niche formation in the gut - modelling growing organoids. FEBS J. 279 (18), 3475–3487. https://doi.org/10.1111/j.1742-4658.2012.08646.x.

Carulli, A.J., Samuelson, L.C., Schnell, S., 2014. Unraveling intestinal stem cell behavior with models of crypt dynamics. Integr. Biol. 6 (3), 243. https://doi.org/10.1039/c3ib40163d.

Chin, A.M., Hill, D.R., Aurora, M., Spence, J.R., 2017. Morphogenesis and maturation of the embryonic and postnatal intestine. Semin. Cell Dev. Biol. 66, 81–93. https://doi.org/10.1016/j.semcdb.2017.01.011.

Clevers, H., 2013. The intestinal crypt, a prototype stem cell compartment. Cell 154 (2), 274–284. https://doi.org/10.1016/j.cell.2013.07.004.

Clevers, H.C., Bevins, C.L., 2013. Paneth cells: maestros of the small intestinal crypts. Annu. Rev. Physiol. 75 (1), 289–311. https://doi.org/10.1146/annurev-physiol-030212-183744.

Ewald, A.J., Brenot, A., Duong, M., Chan, B.S., Werb, Z., 2008. Collective epithelial migration and cell rearrangements drive mammary branching morphogenesis. Dev. Cell 14 (4), 570–581. https://doi.org/10.1016/j.devcel.2008.03.003.

Fatehullah, A., Appleton, P.L., Näthke, I.S., 2013. Cell and tissue polarity in the intestinal tract during tumourigenesis: cells still know the right way up, but tissue organization is lost. Philos. Trans. R. Soc. Lond. B Biol. Sci. 368 (1629), 20130014. https://doi.org/10.1098/rstb.2013.0014.

Gjorevski, N., Sachs, N., Manfrin, A., et al., 2016. Designer matrices for intestinal stem cell and organoid culture. Nature 539 (7630), 560–564. https://doi.org/10.1038/nature20168.

Gregorieff, A., Liu, Y., Inanlou, M.R., Khomchuk, Y., Wrana, J.L., 2015. Yap-dependent reprogramming of Lgr5+ stem cells drives intestinal regeneration and cancer. Nature 526 (7575), 715–718. https://doi.org/10.1038/nature15382.

He, B., Doubrovinski, K., Polyakov, O., Wieschaus, E., 2014. Apical constriction drives tissue-scale hydrodynamic flow to mediate cell elongation. Nature 508 (7496), 392–396. https://doi.org/10.1038/nature13070.

Heuberger, J., Kosel, F., Qi, J., Grossmann, K.S., Rajewsky, K., Birchmeier, W., 2014. Shp2/MAPK signaling controls goblet/paneth cell fate decisions in the intestine. Proc. Natl. Acad. Sci. 111 (9), 3472–3477. https://doi.org/10.1073/pnas.1309342111.

Itzkovitz, S., Blat, I.C., Jacks, T., Clevers, H., van Oudenaarden, A., 2012. Optimality in the development of intestinal crypts. Cell 148 (3), 608–619. https://doi.org/10.1016/j.cell.2011.12.025.

Jodoin, J.N., Coravos, J.S., Chanet, S., et al., 2015. Stable force balance between epithelial cells arises from F-actin turnover. Dev. Cell 35 (6), 685–697. https://doi.org/10.1016/j.devcel.2015.11.018.

Kinoshita, N., Sasai, N., Misaki, K., Yonemura, S., 2008. Apical accumulation of Rho in the neural plate is important for neural plate cell shape change and neural tube formation. Mol. Biol. Cell 19 (5), 2289–2299. https://doi.org/10.1091/mbc.E07-12-1286.

Lee, J.-Y., Harland, R.M., 2007. Actomyosin contractility and microtubules drive apical constriction in Xenopus bottle cells. Dev. Biol. 311 (1), 40–52. https://doi.org/10.1016/j.ydbio.2007.08.010.

Lee, J., Harland, R.M., 2007. Actomyosin contractility and microtubules drive apical constriction in Xenopus bottle cells. Dev. Biol. 311 (1), 40–52. https://doi.org/10.1016/j.ydbio.2007.08.010.

Martin, A.C., Goldstein, B., 2014. Apical constriction: themes and variations on a cellular mechanism driving morphogenesis. Development 141 (10), 1987–1998. https://doi.org/10.1242/dev.102228.

Martin, A.C., Gelbart, M., Fernandez-Gonzalez, R., Kaschube, M., Wieschaus, E.F., 2010. Integration of contractile forces during tissue invagination. J. Cell Biol. 188 (5), 735–749. https://doi.org/10.1083/jcb.200910099.

Nelson, M.R., Howard, D., Jensen, O.E., King, J.R., Rose, F.R.A.J., Waters, S.L., 2011. Growth-induced buckling of an epithelial layer. Biomech. Model. Mechanobiol. 10, 883–900. https://doi.org/10.1007/s10237-010-0280-0.

Nelson, M.R., Howard, D., Jensen, O.E., King, J.R., Rose, F.R.A.J., Waters, S.L., 2011. Growth-induced buckling of an epithelial layer. Biomech. Model. Mechanonbiol. 10, 833–900. https://doi.org/10.1007/s10237-010-0280-0.

Paluch, E., Heisenberg, C.-P., 2009. Biology and physics of cell shape changes in development. Curr. Biol. 19 (17), R790–R799. https://doi.org/10.1016/j.cub.2009.07.029.

Pilot, F., Lecuit, T., 2005. Compartmentalized morphogenesis in epithelia: from cell to tissue shape. Dev. Dynam. 232 (3), 685–694. https://doi.org/10.1002/dvdy.20334.

Razzell, W., Wood, W., Martin, P., 2014. Recapitulation of morphogenetic cell shape changes enables wound re-epithelialisation. Development 141 (9), 1814–1820. https://doi.org/10.1242/dev.107045.

Saias, L., Swoger, J., D'Angelo, A., et al., 2015. Decrease in cell volume generates contractile forces driving dorsal closure. Dev. Cell 33 (5), 611–621. https://doi.org/10.1016/j.devcel.2015.03.016.

Sato, T., Clevers, H., 2012. Primary mouse small intestinal epithelial cell cultures, pp. 319–328. https://doi.org/10.1007/978-1-62703-125-7_19.

Sato, T., van Es, J.H., Snippert, H.J., et al., 2011. Paneth cells constitute the niche for Lgr5 stem cells in intestinal crypts. Nature 469 (7330), 415–418. https://doi.org/10.1038/nature09637.

Sawyer, J.M., Harrell, J.R., Shemer, G., Sullivan-Brown, J., Roh-Johnson, M., Goldstein, B., 2010. Apical constriction: a cell shape change that can drive morphogenesis. Dev. Biol. 341 (1), 5–19. https://doi.org/10.1016/j.ydbio.2009.09.009.

Shyer, A.E., Tallinen, T., Nerurkar, N.L., et al., 2013. Vilification: how the gut gets its villi. Science (80-) 342 (6155), 212–218. https://doi.org/10.1126/science.1238842.

Snippert, H.J., van der Flier, L.G., Sato, T., et al., 2010. Intestinal crypt homeostasis results from neutral competition between symmetrically dividing Lgr5 stem cells. Cell 143 (1), 134–144. https://doi.org/10.1016/j.cell.2010.09.016.

Suzuki, M., Hara, Y., Takagi, C., Yamamoto, T.S., Ueno, N., 2010. MID1 and MID2 are required for Xenopus neural tube closure through the regulation of microtubule organization. Development 137 (14).

Valéry, C., Artzner, F., Paternostre, M., 2011. Peptide nanotubes: molecular organisations, self-assembly mechanisms and applications. Soft Matter 7 (20), 9583. https://doi.org/10.1039/c1sm05698k.

VanDussen, K.L., Carulli, A.J., Keeley, T.M., et al., 2012. Notch signaling modulates proliferation and differentiation of intestinal crypt base columnar stem cells. Development 139 (3), 488–497. https://doi.org/10.1242/dev.070763.

Varner, V.D., Nelson, C.M., 2014. Cellular and physical mechanisms of branching morphogenesis. Development 141 (14), 2750–2759. https://doi.org/10.1242/dev.104794.

Zhao, B., Qi, Z., Li, Y., Wang, C., Fu, W., Chen, Y.-G., 2015. The non-muscle-myosin-II heavy chain Myh9 mediates colitis-induced epithelium injury by restricting Lgr5+ stem cells. Nat. Commun. 6, 7166. https://doi.org/10.1038/ncomms8166.